





# Expression of the wheat multipathogen resistance hexose transporter *Lr67res* is associated with anion fluxes

Ricky J. Milne <sup>1,†</sup> Katherine E. Dibley <sup>1,†</sup> Jayakumar Bose <sup>2,3</sup> Anthony R. Ashton <sup>1</sup> Peter R. Ryan <sup>1</sup>  
Stephen D. Tyerman <sup>2</sup> and Evans S. Lagudah <sup>1,\*</sup>

1 CSIRO, Agriculture and Food, Canberra, ACT 2601, Australia

2 Australian Research Council Centre of Excellence in Plant Energy Biology, School of Agriculture, Food and Wine, University of Adelaide, Urrbrae, SA 5064, Australia

3 School of Science, Western Sydney University, Richmond, NSW 2753, Australia

\*Author for correspondence: evans.lagudah@csiro.au

<sup>†</sup>These authors contributed equally to this work.

The author responsible for distribution of materials integral to the findings presented in this article in accordance with the policy described in the Instructions for Authors (<https://academic.oup.com/plphys/pages/General-Instructions>) is Evans Lagudah.

## Abstract

Many disease resistance genes in wheat (*Triticum aestivum* L.) confer strong resistance to specific pathogen races or strains, and only a small number of genes confer multipathogen resistance. The *Leaf rust resistance 67* (*Lr67*) gene fits into the latter category as it confers partial resistance to multiple biotrophic fungal pathogens in wheat and encodes a Sugar Transport Protein 13 (STP13) family hexose-proton symporter variant. Two mutations (G144R, V387L) in the resistant variant, *Lr67res*, differentiate it from the susceptible *Lr67sus* variant. The molecular function of the *Lr67res* protein is not understood, and this study aimed to broaden our knowledge on this topic. Biophysical analysis of the wheat *Lr67sus* and *Lr67res* protein variants was performed using *Xenopus laevis* oocytes as a heterologous expression system. Oocytes injected with *Lr67sus* displayed properties typically associated with proton-coupled sugar transport proteins—glucose-dependent inward currents, a  $K_m$  of  $110 \pm 10 \mu\text{M}$  glucose, and a substrate selectivity permitting the transport of pentoses and hexoses. By contrast, *Lr67res* induced much larger sugar-independent inward currents in oocytes, implicating an alternative function. Since *Lr67res* is a mutated hexose-proton symporter, the possibility of protons underlying these currents was investigated but rejected. Instead, currents in *Lr67res* oocytes appeared to be dominated by anions. This conclusion was supported by electrophysiology and  $^{36}\text{Cl}^-$  uptake studies and the similarities with oocytes expressing the known chloride channel from *Torpedo marmorata*, *TmClC-0*. This study provides insights into the function of an important disease resistance gene in wheat, which can be used to determine how this gene variant underpins disease resistance *in planta*.

## Introduction

Wheat (*Triticum aestivum* L.) is the major crop grown throughout temperate regions of the world. Many wheat cultivars are susceptible to the disease-causing pathogens

prevalent in these regions. Pathogen infection is the leading biotic cause of grain yield losses, with cumulative global losses due to the three wheat rust diseases—stem rust, leaf rust, and yellow/stripe rust—reaching around US\$2.9 billion

Received November 14, 2022. Accepted January 29, 2023. Advance access publication February 21, 2023

© The Author(s) 2023. Published by Oxford University Press on behalf of American Society of Plant Biologists.

This is an Open Access article distributed under the terms of the Creative Commons Attribution-NonCommercial-NoDerivs licence (<https://creativecommons.org/licenses/by-nc-nd/4.0/>), which permits non-commercial reproduction and distribution of the work, in any medium, provided the original work is not altered or transformed in any way, and that the work is properly cited. For commercial re-use, please contact [journals.permissions@oup.com](mailto:journals.permissions@oup.com)

Open Access

in value annually (Huerta-Espino et al. 2020). The fungal pathogens responsible for these diseases (*Puccinia graminis* f. sp. *tritici*, *P. triticina*, and *P. striiformis* f. sp. *tritici*, respectively) siphon nutrients from infected plants, compromising growth and yield. A chemical-free strategy for controlling fungal diseases utilizes the plant's own disease resistance genes. Strong resistance can be conferred by seedling resistance (R) genes, which recognize pathogen effectors and trigger localized cell death surrounding the infection site, known as the hypersensitive response, thereby preventing pathogen spread to other living tissues. The gene-for-gene interaction between R proteins and pathogen effectors is often pathogen race-specific and may be overcome when a pathogen effector evades R protein recognition. This type of resistance breakdown was exemplified by the emergence of Ug99, a stem rust race group highly virulent against the resistance present in many commercial wheats (Pretorius et al. 2000). There is an ongoing need to discover and introgress new R genes into elite cultivars of wheat to combat the constant evolution of fungal effector proteins. Hence sources of durable resistance are required to protect crops against fungal epidemics.

Adult plant resistance (APR) genes are less common than seedling R genes, and some have the additional desirable characteristic of conferring durable resistance to multiple pathogens. Only a handful of such genes including *Leaf rust resistance 67* (*Lr67*), *Lr34*, and *Lr46* have been described in bread wheat, compared with ~200 race-specific seedling R genes. *Lr67* encodes a sugar transporter orthologous to the *Arabidopsis* (*Arabidopsis thaliana*) Sugar Transport Protein 13 (STP13), *Lr34* encodes an ATP-binding cassette (ABC) transporter, and *Lr46* remains to be fully characterized (Singh et al. 1998; Krattinger et al. 2009; Kolmer et al. 2015; Moore et al. 2015). Unlike race-specific R genes that rely on a gene-for-gene interaction with pathogen avirulence genes, these APR genes confer partial resistance to multiple races of wheat rust and powdery mildew (*Blumeria graminis* f. sp. *tritici*) and are less susceptible to being overcome by the variable nature of obligate pathogen genetics (Ellis et al. 2014). Interestingly, transgenic expression of *Lr34* in other cereals such as barley (*Hordeum vulgare*), rice (*Oryza sativa*), sorghum (*Sorghum bicolor*), and maize (*Zea mays*) confers resistance to fungal pathogens adapted to those particular species (Risk et al. 2013; Krattinger et al. 2016; Schnippenkoetter et al. 2017; Sucher et al. 2017). *Lr67* is anticipated to have the same effect but has only been demonstrated in barley to date (Milne et al. 2019). The mechanism by which APR genes confer resistance is unclear but appears to be fundamentally different from R genes. In bread wheat, APR genes function mainly in adult plants, where they slow pathogen growth in the absence of a hypersensitive response. Since APR genes only confer partial resistance, they can be combined with strong R genes to provide robust and more durable resistance (Ellis et al. 2014).

This study investigated *Lr67* function. Two *Lr67* alleles occur in wheat: the common wild-type *Lr67sus* allele and the rare disease-resistance allele *Lr67res*, distinguished by two

amino acid mutations present in the *Lr67res* variant—G144R and V387L. The G144 residue is highly conserved across sugar porter (SP) family members and the G144R change alone causes the protein to lose its original hexose transport function (Moore et al. 2015). A loss of sugar transport due to introducing the corresponding G144R mutation has also been demonstrated using yeast in other STP13 family transporters, including the barley HvSTP13 and barrel medic (*Medicago truncatula*) MtSTP13.1 (Milne et al. 2019; Gupta et al. 2021) signifying the importance of the highly conserved G144 amino acid for sugar transport. Structural determination of the closely related sugar transport protein AtSTP10 from *Arabidopsis* gives additional insight into the close proximity of the G144 residue to two amino acids involved in proton coupling (D42 and R142 of AtSTP10) (Paulsen et al. 2019; Bavnhoj et al. 2021). It was suggested that the G144R mutation would disrupt the flexibility and charge distribution in this region of the protein, thereby abolishing sugar transport (Bavnhoj et al. 2021). The second mutation present in *Lr67res*, V387L, resides in a less conserved region of the protein, and this mutation alone introduced into *Lr67sus* or HvSTP13 reduced hexose transport in yeast by approximately 50% (Moore et al. 2015; Milne et al. 2019). The region of the protein where the residue corresponds to V387 in AtSTP10 is regarded as being involved with gating of transport (Bavnhoj et al. 2021), hence the observed reduction on sugar transport conferred by the V387L mutation.

In the context of *Lr67res*-mediated disease resistance, HvSTP13<sup>G144R</sup> was expressed as a stable transgene in barley and demonstrated that this mutation alone was sufficient to confer resistance to barley leaf rust caused by the biotrophic fungus *Puccinia hordei* (Skoppek et al. 2022). A disease resistance phenotype has also been extended to a eudicot plant by transiently overexpressing the barrel medic MtSTP13<sup>G144R</sup> in pea (*Pisum sativum*) leaves, resulting in reduced fungal biomass of *Erysiphe pisi*, the biotrophic fungus responsible for pea powdery mildew (Gupta et al. 2021). Interestingly, wild-type STP13 alleles (lacking the G144R mutation) appear to have some role in disease resistance and susceptibility, likely due to sugar partitioning. Overexpression of AtSTP13 in *Arabidopsis* resulted in lower necrotrophic fungal (*Botrytis cinerea*) colonization, and knockdown of AtSTP13 resulted in greater colonization by the same pathogen (Lemonnier et al. 2014). For the *Pseudomonas syringae* bacterial pathogen, multiple STP knockouts were required (both AtSTP13 and AtSTP1) to reduce bacterial colonization, yet, an increase in STP13 hexose transport via phosphorylation mimic mutation resulted in lower bacterial infection (Yamada et al. 2016). In the context of biotrophic pathogens, resistance by knockout/silencing of STP13 did reduce infection; however, this did not appear to be to an equivalent level of resistance as the expression of an *Lr67*-like variant (Huai et al. 2020; Gupta et al. 2021), nor was there any mention of an apparent leaf tip necrosis (Ltn) phenotype in these STP13 knockout/silencing studies. This suggests factors other than sugar partitioning may contribute to *Lr67res* resistance.

Lr67res-mediated disease resistance was proposed to occur via a dominant-negative interference, whereby the non-functional Lr67res protein forms inactive transporter complexes via heterodimerization with the functional STP13 protein homoeologs encoded on the A and B genomes of hexaploid wheat (Moore et al. 2015). The dominant-negative interference hypothesis is based on the Lr67res-mediated reduction of glucose uptake into the cytosol of infected cells, thereby reducing available glucose to support haustorial-feeding pathogen development (Moore et al. 2015). In addition to the redundancy in plant sugar transporter function as evidenced by a normal growth habit and lack of phenotypic abnormalities or Lr67res-associated Ltn phenotype for STP13 knockout plants (Nørholm et al. 2006), further evidence appears to oppose the dominant-negative interference hypothesis. Specifically, a series of chemically induced single amino acid mutations of Lr67res (that retained the G144R and V387L changes) were identified to eliminate disease resistance and Ltn in adult wheat plants (Spielmeyer et al. 2013; Moore et al. 2015). Together, these point toward an alternative function or gain-of-function by Lr67res over the Lr67sus protein, rather than a reduction in sugar transport being responsible for resistance.

Here, we tested the possibility that Lr67res displays an alternative function concurrent with the loss of hexose transport function. To this end, we have generated evidence that the APR Lr67res possesses an alternative function characterized by enhanced ion fluxes that were independent of glucose. We used *Xenopus laevis* oocytes and yeast (*Saccharomyces cerevisiae*) as heterologous expression systems to perform detailed functional characterization studies of both Lr67sus and Lr67res alleles. Since Lr67res is a mutated hexose-proton symporter, the possibility that uncoupling of protons was responsible for the observed currents was thoroughly investigated and appeared not to be the case.

## Results

### Lr67sus mediates proton-hexose symport in *Xenopus* oocytes

To examine functional characteristics of the proteins encoded by Lr67sus and Lr67res, cRNA was injected into *Xenopus* oocytes and analyzed using electrophysiology and isotopic techniques. Lr67sus expression in oocytes induced transport properties typical of other proton-coupled sugar transporters. Specifically, Lr67sus oocytes displayed glucose-dependent inward currents associated with glucose-proton symport, whereas water-injected oocytes did not (Fig. 1A). These glucose-induced currents shifted the oocyte reversal potential from 8 to 33 mV (Fig. 1B), which is consistent with the involvement of protons. The Lr67sus oocytes also accumulated a substantially greater amount of  $^{14}\text{C}$ -glucose than water-injected controls (Fig. 1C). The glucose-dependent currents remained negative and quite linear under these experimental conditions, indicating that

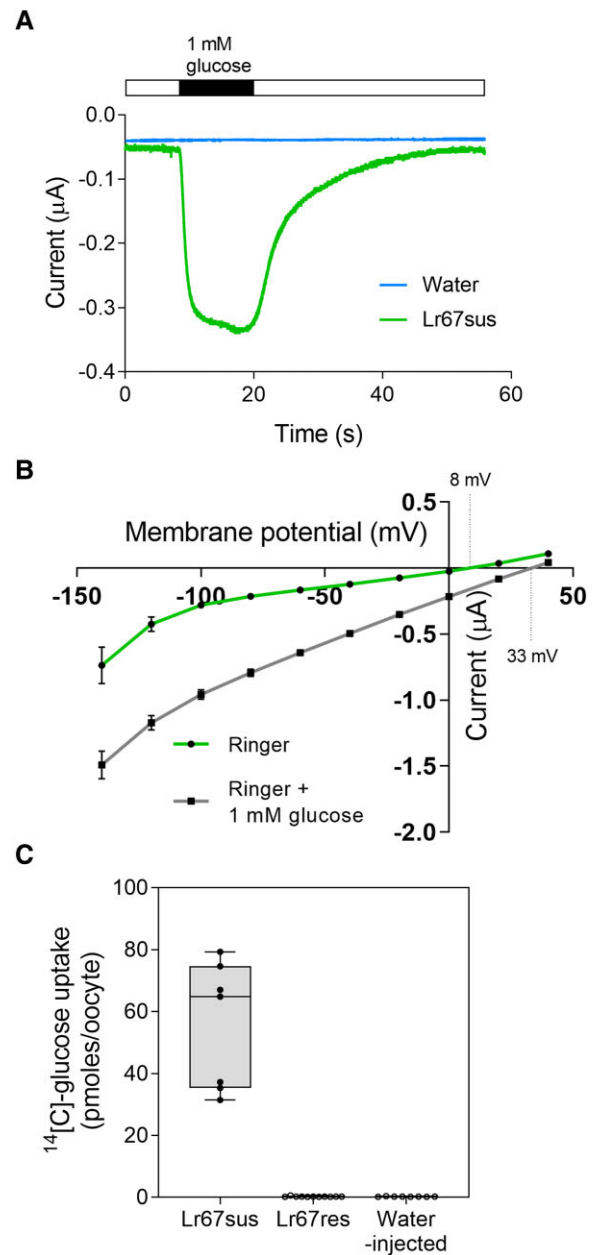


**Figure 1.** Lr67sus transports glucose in *Xenopus* oocytes. **A)** Current trace of single water-injected (upper trace) or Lr67sus-injected (lower trace) oocytes clamped at  $-40$  mV and perfused with 115 mM NaCl Ringer at pH  $5 \pm 1$  mM glucose indicated by the black bar above. **B)** Current–voltage relationship of Lr67sus-injected oocytes under voltage-clamped conditions, perfused with 115 mM NaCl Ringer solution at pH  $5 \pm 1$  mM glucose; dotted lines indicate reversal potential values. Data points with vertical bars represent the mean  $\pm$  SE of seven oocytes. **C)** One-hour glucose uptake by oocytes injected with Lr67sus, Lr67res, or water, incubated in 115 mM NaCl Ringer at pH 5 containing  $11.4 \mu\text{M}$   $^{14}\text{C}$ -glucose. Elements of box and whisker plot—center line, median; box limits, 25th and 75th percentiles; whiskers, max and min values; points, all data points;  $n = 7$  to 11 oocytes.

glucose transport activity was not voltage dependent (Supplemental Fig. S1). Transport assays over a range of glucose concentrations revealed Michaelis–Menten-like

saturation kinetics with an apparent  $K_m$  of  $110 \pm 10 \mu\text{M}$  glucose at  $-120 \text{ mV}$  (Fig. 2A) which is close to the  $K_m$  determined for Lr67sus in yeast ( $99 \mu\text{M}$  glucose; Moore et al. 2015) and to the glucose affinities of closely related members of the STP13 transporter family from tomato (LeHT2,  $45 \mu\text{M}$ ), Arabidopsis (AtSTP13,  $74 \mu\text{M}$ ), and grapevine (VvHT5,  $89 \mu\text{M}$ ) (Gear et al. 2000; Nørholm et al. 2006; Hayes et al. 2007). In contrast to glucose transport activity, the  $K_m$  for glucose was voltage-dependent (Fig. 2B). Lr67sus showed a strong substrate selectivity for pentoses and hexoses compared with sugar alcohols, disaccharides or the trisaccharide raffinose, which were not transported (Fig. 3). When membrane voltage remained unclamped, the addition of  $1 \text{ mM}$  glucose (pH 4.5) to Lr67sus oocytes caused the membrane to depolarize by  $\sim 50 \text{ mV}$  which was 2-fold greater than a pH 4.5 solution without glucose (Fig. 4A). Addition of  $1 \text{ mM}$  glucose (pH 4.5) also acidified the cytosol to a greater extent than a pH 4.5 solution alone (Fig. 4B). These sugar-induced changes in the membrane potential and cytosolic pH of Lr67sus oocytes were greater than those in the water-injected controls. Such measurements have not yet been

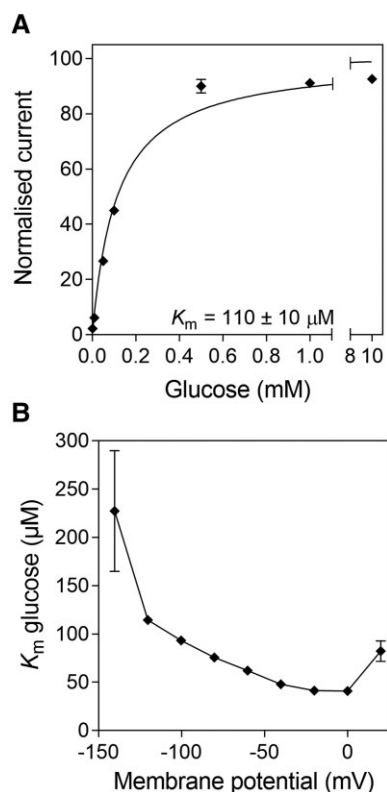


**Figure 2.** Glucose affinity of Lr67sus in *Xenopus* oocytes. **A)** Kinetic analysis of glucose transport by Lr67sus-injected oocytes under voltage-clamped conditions at a membrane potential of  $-120 \text{ mV}$ . A Michaelis–Menten curve was fitted which was then normalized to  $V_{\text{max}}$  and plotted against the substrate concentration. **B)** Voltage dependence of Lr67sus glucose  $K_m$  at membrane potential values from  $-140$  to  $20 \text{ mV}$ . Data points with vertical bars in (A) and (B) represent the mean  $\pm$  SE of 4 oocytes.

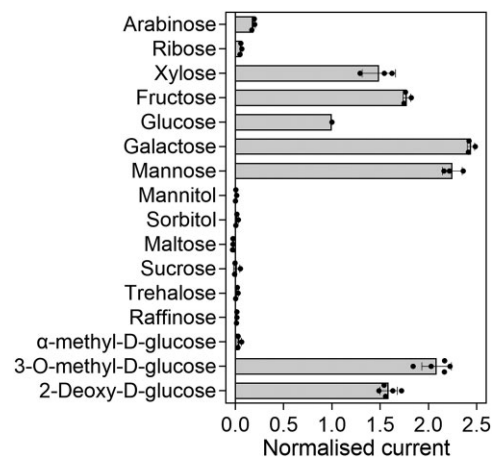


**Figure 3.** Substrate selectivity of Lr67sus-injected oocytes. Substrates at a concentration of  $5 \text{ mM}$  were applied to oocytes in a  $115 \text{ mM}$  NaCl Ringer solution and induced currents were measured at a membrane potential of  $-120 \text{ mV}$ . Substrate-induced currents were normalized to the current induced by  $5 \text{ mM}$  glucose of the same oocyte. Columns with horizontal bars represent the mean  $\pm$  SE of 3 to 5 oocytes.

reported for STP expression in oocytes; however, our observations are typical of oocytes expressing more distantly related proton-coupled sucrose transporters from the SUT family (belonging to the major facilitator superfamily but distinct to STPs) (Reinders et al. 2008; Sun et al. 2010).

### Lr67res does not transport glucose but induces glucose-independent ion currents in *Xenopus* oocytes

In contrast to Lr67sus, the expression of Lr67res in oocytes did not increase  $^{14}\text{C}$ -glucose uptake (Fig. 1C) and the addition of glucose to non-voltage-clamped oocytes did not depolarize the membrane (Fig. 4A) or shift the reversal potential in voltage-clamped oocytes (Fig. 5A). Instead, Lr67res expression induced large glucose-independent currents that reversed near  $-30 \text{ mV}$  (Fig. 5, A and B). The magnitude of these currents was  $\sim 10$ -fold greater than the glucose-dependent currents measured in Lr67sus oocytes (Fig. 1B). Given that Lr67res is a mutated glucose-proton symporter, the possibility that proton fluxes underlie these large currents was investigated by changing the pH of the bathing medium and measuring changes in both cytosolic pH and membrane potential. In  $115 \text{ mM}$  NaCl Ringer solution (pH 7.6), the cytosolic pH of Lr67res oocytes was more alkaline than the water-injected controls while cytosolic pH of Lr67sus oocytes was more acidic than controls. Nevertheless, the changes in cytosolic proton concentration caused by shifting bathing solution pH from 7.6 to 4.5 was similar for all oocytes (Fig. 4B; Supplemental Fig. S2). Unlike Lr67sus and control oocytes, which both showed large shifts in membrane potentials as the external pH and glucose concentrations were changed, the membrane potential of Lr67res oocytes changed little and remained near  $-20 \text{ mV}$

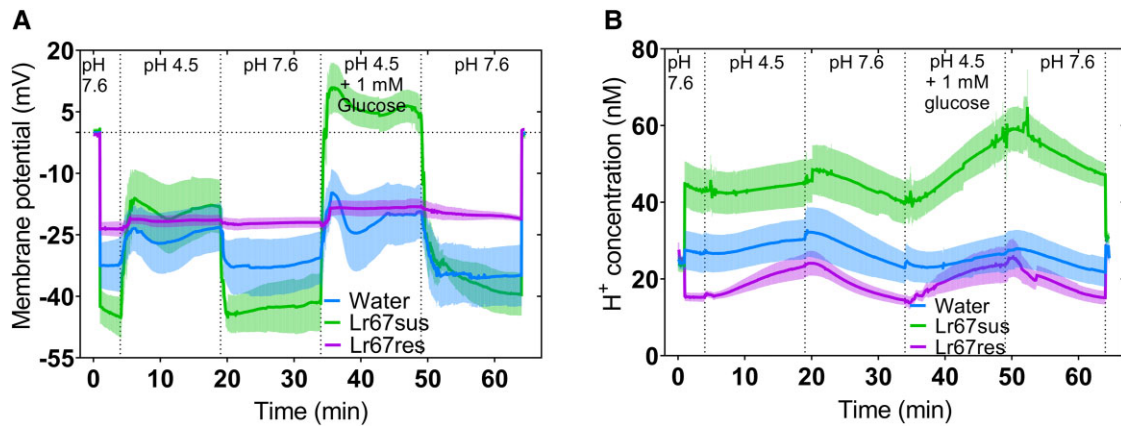


**Figure 4.** Effect of changing external pH on membrane potential and cytosolic H<sup>+</sup> concentration of oocytes injected with *Lr67* alleles. **A)** Membrane potential and **B)** Cytosolic H<sup>+</sup> concentration of *Lr67sus*, *Lr67res* or water-injected oocytes exposed to 115 mM NaCl Ringer solution with different pH values and glucose concentrations. Dark traces with light shading in (A) and (B) represent the mean  $\pm$  SE of 5 to 6 oocytes.

for those treatments (Fig. 4B). This response was confirmed in voltage-clamped *Lr67res* oocytes because reducing pH of the bathing solution induced larger inward currents without shifting the reversal potential (Fig. 5C). Changing the bathing solution from pH 8 to pH 4 with control oocytes induced much smaller current changes but shifted the reversal potential in the positive direction by 36 mV (from  $-29$  to  $+7$  mV; Supplemental Fig. S3A). The absence of any depolarization in *Lr67res* oocytes as pH of the bathing solution was decreased together with the absence of any shift of reversal potential in voltage-clamped oocytes, indicates that protons were not a major contributor to the large currents (Figs. 4A and 5C). Instead, the results indicate that *Lr67res* oocytes were more permeable to one or more other ions that clamped the membrane potential between  $-20$  and  $-30$  mV.

### Currents in *Lr67res* oocytes appear to be anion-dominated

To investigate the identity of the large currents in *Lr67res* oocytes in more detail, we first varied the NaCl concentration in the oocyte bathing solution. As external NaCl concentration was changed from 10 to 115 mM, the current magnitudes increased by  $\sim 5$   $\mu$ A (at  $-140$  mV) and the reversal potential shifted from  $-1$  to  $-30$  mV (Fig. 5A). This negative shift in reversal potential by  $-29$  mV more closely tracks the equilibrium potential for Cl<sup>-</sup> rather than Na<sup>+</sup>. Indeed, previous studies have demonstrated that increasing external NaCl causes positive shifts in reversal potential for oocytes expressing transporters that are permeable to Na<sup>+</sup> (Uozumi et al. 2000; Munns et al. 2012). The control oocytes showed much smaller changes in membrane potential ( $-6$  mV) and current ( $-0.5$   $\mu$ A at  $-140$  mV) when external NaCl was increased (Supplemental Fig. S3B). Although these results indicate that Na<sup>+</sup> fluxes were not dominating the currents, the final Na<sup>+</sup> concentration in *Lr67res*-injected oocytes was  $\sim 60\%$  greater than *Lr67sus* or water-injected oocytes (Fig. 6A).

The large currents in *Lr67res* oocytes were investigated further by additional changes to the oocyte bathing solution. Substituting Na<sup>+</sup> with K<sup>+</sup> or choline<sup>+</sup>, whilst maintaining a constant Cl<sup>-</sup> concentration, had no effect on the current magnitudes or reversal potentials (Fig. 6B; Supplemental Table S1). The same substitutions in control oocytes revealed no change in the current magnitude, and a shift in reversal potential of 4 mV ( $-6$  to  $-2$  mV) was observed when Cl<sup>-</sup> was substituted for gluconate<sup>+</sup> (Supplemental Fig. S3C and Supplemental Table S1). By contrast, substituting Cl<sup>-</sup> for gluconate<sup>-</sup> or NO<sub>3</sub><sup>-</sup> did induce changes to both the current magnitudes and reversal potentials. For instance, substituting Cl<sup>-</sup> with the less-permeable anion, gluconate<sup>-</sup>, reduced the current magnitude and shifted the reversal potential in the positive direction by 52 mV, from  $-26$  to  $+26$  mV (Fig. 6B). By contrast, substituting Cl<sup>-</sup> with NO<sub>3</sub><sup>-</sup>, another permeable anion, increased the outward current (equivalent to anion influx) and shifted the reversal potential from  $-22$  to  $-42$  mV (Fig. 6C). This shift in reversal potential tracks the predicted equilibrium potential for NO<sub>3</sub><sup>-</sup>, given a cytosolic NO<sub>3</sub><sup>-</sup> concentration in oocytes of  $<1$  mM (Liu et al. 1999; Liu and Tsay 2003). A negative shift in reversal potential of  $-18$  mV (from  $-19$  to  $-37$  mV) was observed in control oocytes by substituting Cl<sup>-</sup> for NO<sub>3</sub><sup>-</sup>, however no change in current magnitude was observed (Supplemental Fig. S3D and Supplemental Table S1). NO<sub>3</sub><sup>-</sup> and gluconate<sup>-</sup> were tested in these experiments because, in heterologous expression systems, many plant anion channels are permeable to anions that may not necessarily be their primary substrate *in planta* (Kollist et al. 2011; Wang et al. 2012).

The function of *Lr67res* in oocytes was then compared with ClC-0, the known Cl<sup>-</sup> channel from *Torpedo marmorata* (Jentsch et al. 1990). As found for *Lr67res* oocytes, ClC-0 expression in oocytes generated large glucose-independent currents that reversed near  $-30$  mV, which is close to the predicted equilibrium potential for Cl<sup>-</sup> (Weber 1999) (Supplemental Fig. S4). Furthermore, changing bathing

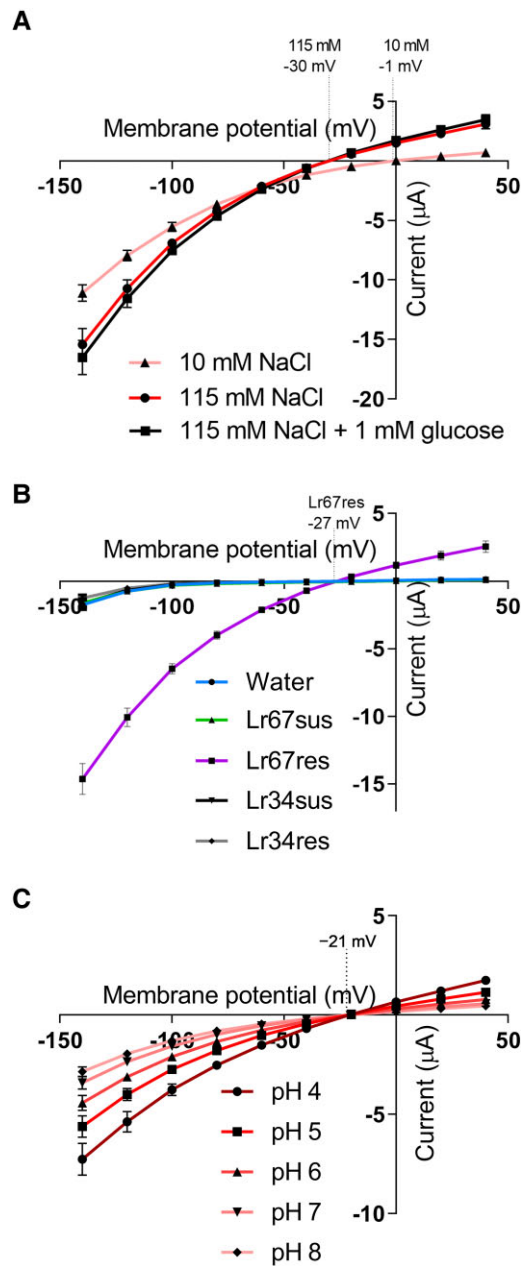


**Figure 5.** Comparing APR alleles and testing the effect of NaCl, glucose and external pH on *Lr67res* oocytes. **A)** Current–voltage relationship of *Lr67res*-injected oocytes perfused with 10 mM NaCl Ringer solution or 115 mM NaCl Ringer solution  $\pm$  1 mM glucose. **B)** Current–voltage relationship of oocytes injected with water, *Lr67sus*, *Lr67res*, *Lr34sus* or *Lr34res*, perfused with 115 mM NaCl Ringer solution. **C)** *Lr67res*-injected oocytes perfused with 115 mM NaCl Ringer solution at pH values from pH 4 to pH 8. Agar bridges were used as bath electrodes in (A). Dotted lines indicate reversal potential values. Data points with vertical bars in (A)–(C) represent the mean  $\pm$  SE of 4 to 11 oocytes.

solution pH from 7.6 to 4.5 was not associated with changes in membrane potential for *Lr67res* as found for the *Lr67res* oocytes (Supplemental Fig. S5). The currents in *Lr67res* oocytes were sensitive to phlorizin (Fig. 6D), a known inhibitor

of *Lr67sus* (Moore et al. 2015) and other sugar transporters, whilst the currents in *CIC-0* and water-injected control oocytes were unaffected by phlorizin (Supplemental Fig. S4). This suggests that the *Lr67res* protein contributed to the observed large currents. Finally, the contribution of anion fluxes to the current was further supported by radio-tracer experiments which found that  $^{36}\text{Cl}^-$  uptake by *Lr67res* and *CIC-0*-injected oocytes was comparable and much greater than those measured in *Lr67sus* oocytes and water-injected controls (Fig. 6E).

### Analysis of *Lr67res* loss-of-resistance mutants

A series of eight chemically induced mutants that caused a loss-of-resistance (LOR) in *Lr67res* plants were previously described in wheat and the majority of these were single amino acid mutations within the *Lr67res* gene (Spielmeyer et al. 2013; Moore et al. 2015). A subset of four of these mutants with single amino acid substitutions were examined in this study—*Lr67res*<sup>C75Y</sup>, *Lr67res*<sup>E160K</sup>, *Lr67res*<sup>G208D</sup>, and *Lr67res*<sup>G217D</sup> (Fig. 7A). These single amino acid mutations of *Lr67res*, whilst G144R and V387L mutations were retained, caused a loss of *Lr67res*-mediated resistance in wheat and a loss of the Ltn phenotype. These LORs were examined in an attempt to associate disease resistance *in planta* with the phenotypes detected in oocytes and yeast. When expressed in yeast these LOR mutants did not restore glucose transport capacity (Fig. 7B). Co-expression of *Lr67sus* in yeast with either *Lr67res*, *Lr67res*<sup>C75Y</sup>, or *Lr67res*<sup>G208D</sup> resulted in ~50% lower glucose uptake compared to *Lr67sus* alone (Fig. 7C). *Lr67sus* glucose uptake was unaffected by co-transformation with an empty vector, most likely because the empty vector did not produce any protein (Fig. 7C). Further, when either the *Lr67res*<sup>C75Y</sup> or *Lr67res*<sup>G208D</sup> LOR mutants were expressed in oocytes, the large currents typically associated with *Lr67res* were absent (Fig. 7D), thus providing an association between the observed *Lr67res* function phenotype in oocytes (large inward currents) with disease resistance *in planta*.

### Discussion

Few plant transporters from the STP family have been characterized using *X. laevis* oocytes, especially where two-electrode voltage-clamp (TEVC) methodology is employed, so this study provides an important insight into both the wheat *Lr67sus* protein which functions as a hexose-proton symporter, and the rare *Lr67res* variant that does not transport glucose but is associated with enhanced ion fluxes in oocytes. *Lr67sus* displayed similar characteristics to closely related hexose-proton symporters, supporting a role in hexose retrieval from the apoplasm (Slewiniski 2011). Since STP13 is known to be responsive both biotic and abiotic stresses (e.g. cold, osmotic, drought, salt stress, wounding) (Nørholm et al. 2006; Hayes et al. 2010; Yamada et al. 2011, 2016) it is proposed to function in mobilization and/or recovery of hexoses under stressful conditions. In hexaploid

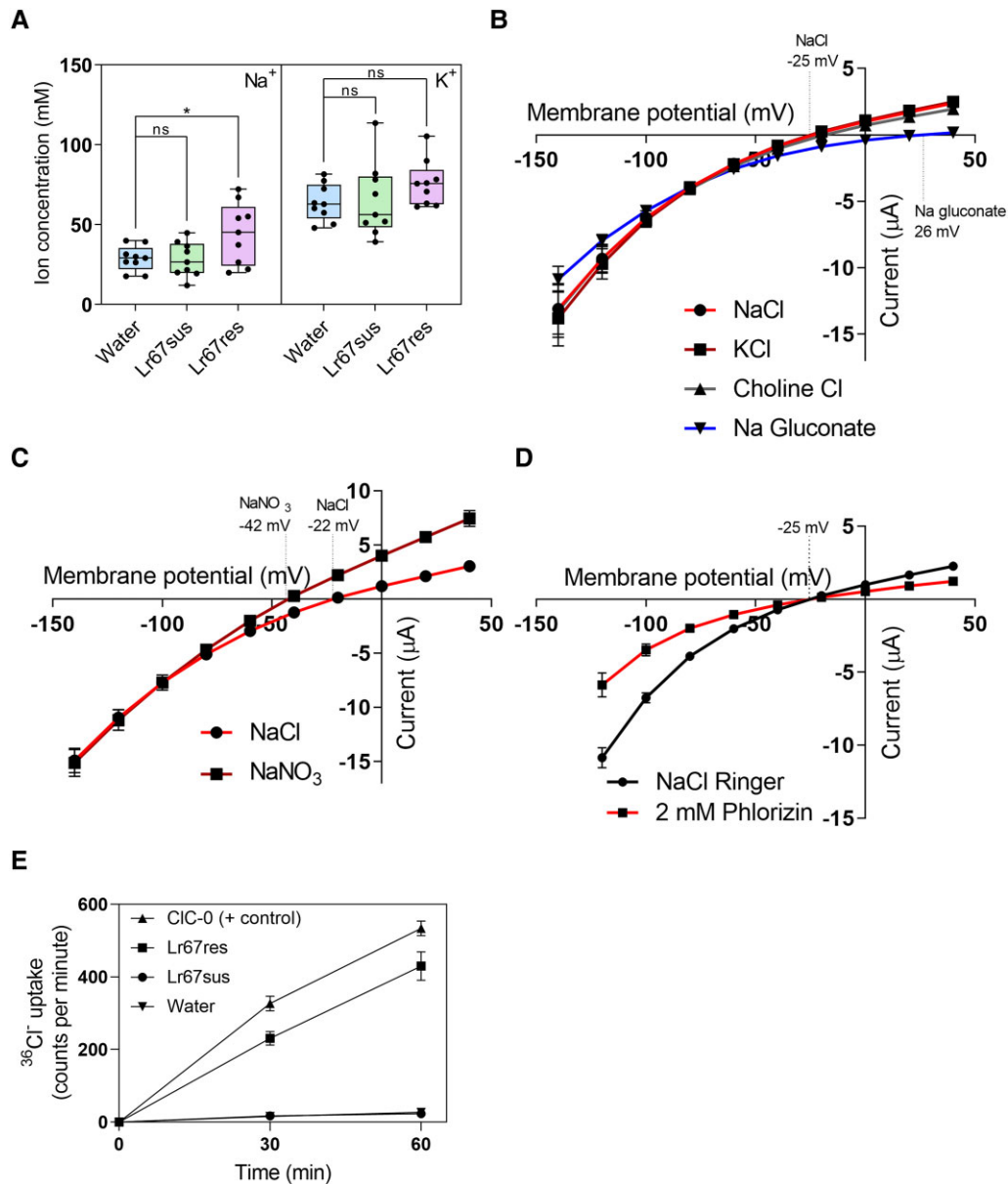


**Figure 6.** Characterizing the Lr67res function in oocytes. **A**) Na<sup>+</sup> and K<sup>+</sup> content of oocytes injected with *Lr67sus*, *Lr67res*, or water, bathed in ND96 solution with antibiotics for 48 h post-injection; \**P* < 0.05 (*T*-test comparing *Lr67* alleles with water control); ns, not significant. Elements of box and whisker plot—center line, median; box limits, 25th and 75th percentiles; whiskers, max and min values; points, all data points; *n* = 9 pooled oocyte samples. **B, C**) Current–voltage relationship of *Lr67res*-injected oocytes perfused with different solutions as indicated. **D**) Current–voltage relationship of *Lr67res*-injected oocytes perfused 115 mM NaCl Ringer ± 30-second 2 mM phlorizin treatment. **E**) Time-course uptake of radiolabeled <sup>36</sup>Cl<sup>-</sup> into injected oocytes as indicated, bathed in ND96 without antibiotics at pH 5.5. Dotted lines in (B)–(D) indicate reversal potentials of the currents. Agar bridges were used as bath electrodes in (B) and (C). Data points with vertical bars represent the mean ± SE of 5–8 oocytes (B)–(D) or 9 to 10 oocytes (E).

wheat, a partial or complete deletion of the *Lr67sus* gene did not appear to impact plant development (Moore et al. 2015) presumably due to redundancy in the STP family as also evidenced in *Arabidopsis*, by the lack of observable phenotype in *stp13* knockout plants (Nørholm et al. 2006). Here, the possibility of an alternative function conferred by *Lr67res* is discussed along with the likelihood of this contributing to disease resistance in *planta*.

### Considering the feasibility of a sugar transporter associated with ion fluxes

Evidence generated in this study suggests that the *Lr67res* variant may confer an alternative function that changes the permeability of the oocyte plasma membrane to small ions. The observed shifts in oocyte reversal potential (Fig. 6, B and C) and the close parallels with observed properties of the well-characterized Cl<sup>-</sup> channel TmCIC-0 (Fig. 6E;

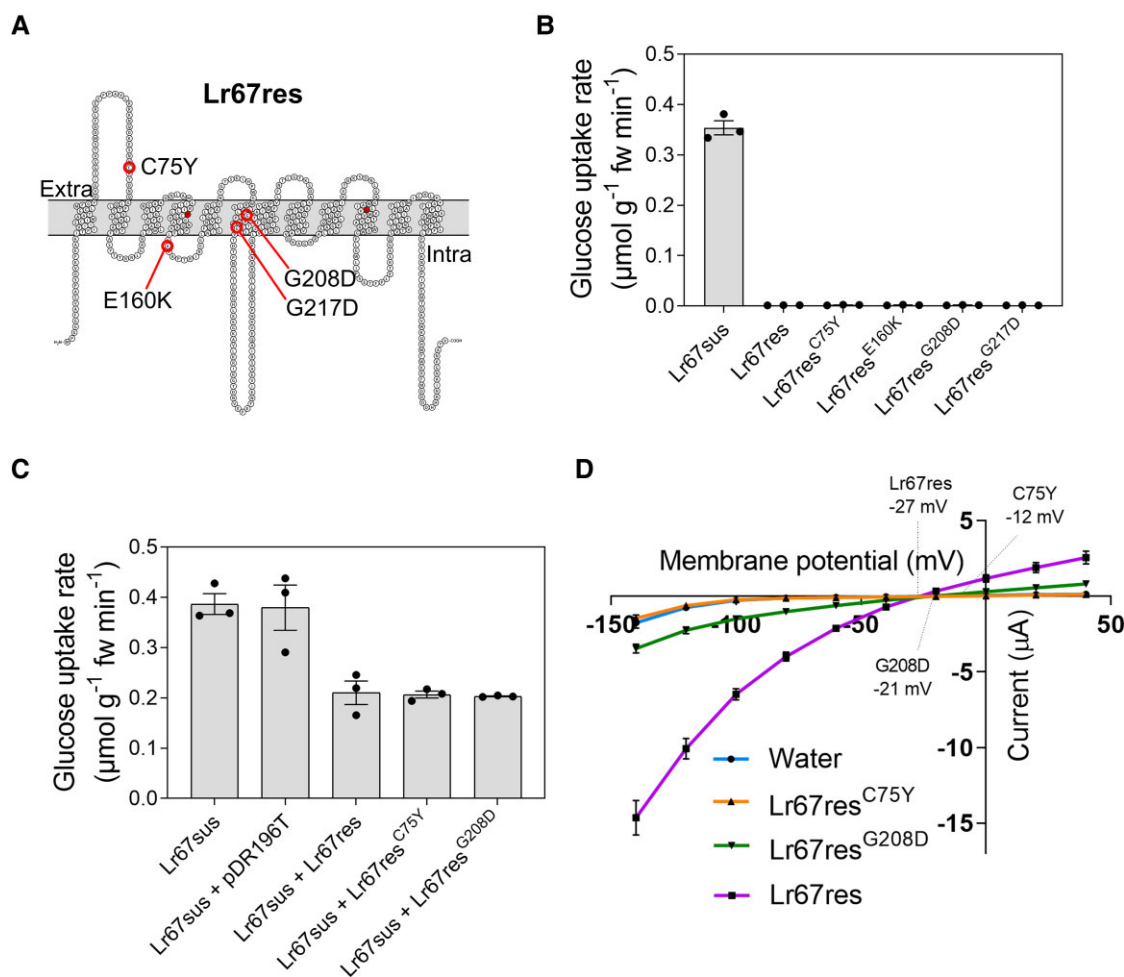


**Figure 7.** Lr67res LOR mutants do not transport glucose and lack Lr67res-associated large inward currents. **A)** Predicted transmembrane topology plot highlighting four single amino acid changes that cause a LOR phenotype in *Lr67res* wheat (Moore et al. 2015), extracellular and intracellular domains are indicated along with G144R and V387L. **B)** Four-minute [ $^{14}\text{C}$ ]-glucose uptake into EBY.VW4000 yeast transformed with *Lr67sus*, *Lr67res* or each mutant shown in (A). **C)** Four-minute [ $^{14}\text{C}$ ]-glucose uptake of yeast transformed with *Lr67sus* alone or *Lr67sus* co-transformed with the pDR196T empty vector, *Lr67res* or LOR mutants as indicated. **D)** Current–voltage relationship of *Xenopus* oocytes perfused with 115 mM NaCl Ringer solution under voltage-clamped conditions, injected with water, *Lr67res*, *Lr67res*<sup>C75Y</sup> or *Lr67res*<sup>G208D</sup>. Dotted lines in (D) indicate reversal potentials of the currents. Columns with vertical bars (B, C) represent mean  $\pm$  SE of three biological replicates (independently transformed yeast colonies). Data points with vertical bars (D) represent the mean  $\pm$  SE of 5 to 8 oocytes.

Supplemental Figs. S4 and S5) provide evidence that anion fluxes, particularly  $\text{Cl}^-$  or  $\text{NO}_3^-$ , may account for the currents observed in Lr67res oocytes. While it is impossible to eliminate the involvement of endogenous oocyte transporters in mediating this flux, the inhibition of currents by the sugar transporter inhibitor phlorizin (Fig. 6D) is consistent with Lr67res contributing to the observed currents, with the caveat that phlorizin may disrupt Lr67res interaction with, or activation of, endogenous oocyte transporters. We closely examined the prospect of observed oocyte currents being a product of uncoupled flux of protons through Lr67res, however the hallmarks of proton flux that were observed for the functional Lr67sus glucose-proton symporter (Fig. 1B) were absent for Lr67res (Fig. 5A). Thus, we concluded that protons are unlikely

to be responsible for the observed current, and this is discussed in more detail below.

It is conceivable that mutation of the highly conserved G144 residue of Lr67 does indeed confer an alternative function and simultaneous loss of sugar transport function, given observations from previous studies. Most notable of these are recent reports of a transient  $\text{Cl}^-$  binding site identified in the crystal structure of an inward-open conformation of the closely related AtSTP10 (Bavnhøj et al. 2021) and the more phylogenetically distant glucose transporter GLUT1 (Custódio et al. 2021). We suggest that the G144R mutation of Lr67res may enable the transit of this bound  $\text{Cl}^-$  through the transporter, giving rise to the alternative function reported in our study. Additionally, the Lr67res G144R mutation is found one helical turn from conserved arginine and



aspartate residues of the structurally resolved XylE (Arg133, Asp27) and AtSTP10 (Arg142, Asp42) that constitute the proton-binding site of each transporter (Sun et al. 2012; Paulsen et al. 2019). The protonation/deprotonation of this pair is thought to drive the conformational change that drives hexose transport (Wisedchaisri et al. 2014). The close proximity of G144R to these critical residues within the predicted 3D structure of Lr67res supports our observations of Lr67res having an alternative function. There are also precedents for single residue mutations, or a 4-residue deletion in the case of hGLUT1 (Weber et al. 2008), in transporters beyond the SP family substantially altering the protein function. For instance, single residue mutations can uncouple the transport of substrates from their co-transported ions (Borre and Kanner 2004; Martial et al. 2006), or induce novel properties that allow the passage of previously excluded ions (Meredith 2004; Bruce et al. 2005; Weber et al. 2008; Qin and Boron 2013). Also of particular relevance is that a single amino acid mutation in the proton-pumping bacteriorhodopsin converts it from a proton pump to a Cl<sup>-</sup> pump (Sasaki et al. 1995).

### Neither proton or a loss of glucose transport are likely to underpin Lr67res disease resistance

As Lr67sus is a proton-coupled hexose transporter, the possibility of a simple uncoupling of glucose and proton transport for Lr67res was closely examined. We showed that glucose uptake by Lr67sus-injected oocytes was associated with glucose-induced inward currents, glucose, and pH-dependent shifts in reversal potential and cytosolic acidification (Figs. 1A and 4B), confirming that proton fluxes were detectable in the *Xenopus* oocyte expression system. The lack of glucose uptake by Lr67res-injected oocytes (Fig. 1C) agrees with previous observations in yeast (Moore et al. 2015), and no differences in the rate of cytosolic acidification between Lr67sus, Lr67res or control oocytes when external pH was acidified (Fig. 4B; Supplemental Fig. S2). However, the increase of current magnitude in acidic solutions in the absence of concurrent shift in reversal potential (Fig. 5C) suggests the possibility of proton transport cannot be eliminated, but we conclude that protons are unlikely to be a major contributor to the large observed current in Lr67res oocytes. Despite this, it is possible that external pH physically alters the geometry or charge density of the outer face of the Lr67res protein which influences the transport rate. Although Lr67res-injected oocytes accumulated more Na<sup>+</sup>, electrophysiological studies indicated that other cations were not a major contributor to the currents either—the minor changes in the current magnitude when Na<sup>+</sup> was substituted for K<sup>+</sup> or choline<sup>+</sup> and by the shifts in reversal potential associated with changing external NaCl concentration were more consistent with anion permeability. Furthermore, the currents measured in Lr67res oocytes contrasted with those induced by the expression of two known Na<sup>+</sup> transporters, TaHKT1; 5-A and AtHKT1. These proteins caused a positive shift in reversal potential as external Na<sup>+</sup>

was increased (Uozumi et al. 2000; Munns et al. 2012), whereas a negative shift was observed in Lr67res oocytes. To reconcile the Lr67res-induced NaCl accumulation (Fig. 6A) coupled with anion fluxes in oocytes (Fig. 6E), we propose that under high external NaCl, the uptake of Cl<sup>-</sup> by Lr67res triggers the uptake of Na<sup>+</sup> to maintain electroneutrality. It was observed that the viability of Lr67res oocytes rapidly declined 2 days post-injection (dpi) in comparison with Lr67sus and water-injected oocytes that had much greater survival. It, therefore, may be possible that the accumulation of Na<sup>+</sup> continues until it becomes toxic. Examining oocyte survival rate in solutions with a range of Na<sup>+</sup> and anion concentrations may be a useful strategy to determine whether this is indeed a contributing factor.

Our experimental evidence does not support the model of a loss of glucose transport function by Lr67res underpinning disease resistance. Firstly, mutations of Lr67res that caused a LOR *in planta* (C75Y, E160K, G208D, G217D) (Spielmeyer et al. 2013; Moore et al. 2015) did not restore glucose transport by Lr67res *in vitro* (Fig. 7, A and B). Secondly, yeast glucose uptake experiments carried out that led to the dominant-negative interference hypothesis were based on a reduction of yeast glucose uptake when Lr67res was co-expressed with the functional Lr67sus, or functional STP13s encoded by homoeologues situated on the A or B genome of hexaploidy wheat (Moore et al. 2015). These experiments lacked important controls included here that demonstrated no reduction in yeast glucose uptake occurred when Lr67sus was co-transformed with an empty vector. However, when Lr67sus was co-expressed with an LOR mutant or Lr67res, the same reduction on glucose transport occurred (Fig. 7C), despite the LOR mutants not conferring resistance *in wheat*. Together, these results indicate that *in planta* resistance is unlikely to be caused by a dominant-negative interference of glucose uptake, as proposed previously (Moore et al. 2015). Further, the reduction in Lr67res oocyte currents by LOR mutations (Fig. 7D) gives support to associate the Lr67res function with resistance.

In the context of disease resistance, anion fluxes, and in particular Cl<sup>-</sup>, have been implicated in immune signaling (Liu et al. 2019), with evidence accumulating of Cl<sup>-</sup> channels and transporters being both positive (Han et al. 2019) and negative (Guo et al. 2014) regulators of PAMP- and effector-triggered immunity. The occurrence of Ltn in plants carrying Lr67res in the absence of pathogen infection (Moore et al. 2015; Milne et al. 2019) indicates that physiological changes leading to resistance are not necessarily reliant on pathogen induction. Instead, we propose that Lr67res-associated ion fluxes *in planta* underpin both multipathogen resistance and the observed Ltn induction, and future experiments will work toward characterizing whether these phenotypic responses are due to localized perturbations in ion distribution or more systemic ion-induced abiotic stress signaling. In contrast to the classical immune response involving gene-for-gene recognition which has recently been linked to calcium ion permeability culminating

in the hypersensitive response and cell death (Bi et al. 2021; Jacob et al. 2021), the partial multipathogen resistance and durability of *Lr67res* could instead rely on changes to ion permeability of the host cell's plasma membrane, rendering the host tissues less conducive to pathogen growth and virulence, in the absence of the hypersensitive response, through an as yet unidentified mechanism.

### Prospects for novel disease resistance by engineering STP13 variants

The G144R amino acid substitution of STP13 was found to be the sole requirement for conferral of *Lr67res*-like rust resistance in barley (Skoppek et al. 2022), and powdery mildew resistance when a barrel medic *STP13<sup>G144R</sup>* variant was transiently expressed in pea leaves (Gupta et al. 2021). This finding in pea is important since it appears that *Lr67*-like resistance is not confined to cereals and the high conservation of STP13 across plant species makes it a valuable, uncomplicated target for gene editing. This is in stark contrast to another wheat multipathogen APR gene, *Lr34*, which encodes an ABC transporter. Unlike *Lr67*, *Lr34* was demonstrated to transport the plant hormone ABA (Krattinger et al. 2019) and given that oocytes injected with *Lr34sus* and *Lr34res* alleles did not display large inward currents like *Lr67res* oocytes (Fig. 5B), their respective molecular functions appear distinct despite similar partial disease resistance in wheat coupled to Ltn. The disease resistance function of *Lr34* is transferrable to other cereals such as barley, rice, sorghum, and maize using the wheat *Lr34res* as a stable transgene (Risk et al. 2013; Krattinger et al. 2016; Schnippenkoetter et al. 2017; Sucher et al. 2017), however unlike *Lr67*, there does not appear to be clear *Lr34* orthologues in plant species outside wheat. Introducing the corresponding mutations to those present in the *Lr34res* transporter into the most closely related sorghum protein (Sb01g016775<sup>ΔF525, Y613H</sup>) did not result in disease resistance in sorghum (Schnippenkoetter et al. 2017). Therefore, STP13 indeed represents a much more straightforward target for crop improvement.

Pinpointing naturally occurring mutants in target crop species is a logical starting point to circumvent regulatory issues around GM and/or gene editing. The G144R substitution is rare in wheat genotypes and was not identified in diverse accessions of barley (Milne et al. 2019). If naturally occurring *Lr67*-like variants in other crops are also rare or undetectable, chemical mutagenesis could be a logical, albeit labor intensive, step to develop novel sources of nontransgenic resistance. Due to sequence conservation within the STP13 gene of many plant species, a GC→CG base pair transversion is required to change the codon encoding the conserved glycine to an arginine (sequence alignment shown in Supplemental Fig. S6). However, the equivalent G144R change is unlikely to be readily achieved via the commonly used chemical mutagen ethylmethyl sulfonate treatment since this treatment generally favors GC→TA base pairs transversions (e.g. in plants, see Greene et al. 2003; Till

et al. 2007). Therefore, a gene editing approach based on prime editing (for review, see Li et al. 2021) would likely be the most safe and efficient method to introduce an *Lr67*-like allele into crops.

Regardless of the approach used to introduce *Lr67res*-like variants in other crops, pleiotropic effects of this gene variant must also be overcome. These pleiotropic effects are minimal in wheat and are largely limited to Ltn (Moore et al. 2015), but were much more severe when the wheat *Lr67res* gene was stably transformed into barley (Milne et al. 2019). It is unknown whether the pleiotropic effects observed in barley transgenics were minimized by using the native barley STP13 sequence containing the G144R mutation as a transgene (Skoppek et al. 2022), however a strategy used for *Lr34res* which also confers pleiotropic effects when expressed as a transgene in barley (Risk et al. 2013) and other crops, was to drive expression using a pathogen-inducible promoter (Boni et al. 2018). Developing a better understanding of how APRs such as *Lr67* and *Lr34* function will greatly improve prospects of transferring useful multipathogen resistance into a range of crop species.

In summary, we functionally characterized the *Lr67sus* and *Lr67res* alleles using *Xenopus* oocytes. Whilst *Lr67sus* displayed functional properties typical of a proton-coupled hexose transporter, an alternative or gain-of-function was associated with *Lr67res* oocytes, resulting in an increased permeability to anions. Although more work is required to refine nuances of the *Lr67res* transport mechanism, this study provides detailed characterization of the *Lr67res* function and represents a substantial step toward understanding multipathogen resistance in crops.

## Materials and methods

### Constructs for yeast and oocyte expression

The full-length coding sequences of *Lr67* and *Lr34* alleles were PCR amplified and cloned into the pENTR1A entry vector (Life Technologies, Mulgrave, VIC, Australia) using specified primers and restriction sites (Supplemental Table S2). Site-directed mutagenesis was used to introduce C75Y, E160K, G208D, and G217D mutations into *Lr67res* using primers in Supplemental Table S2, designed by the QuikChange webpage—<https://www.genomics.agilent.com/primerDesignProgram.jsp> using the protocol as described for *HvSTP13* (Milne et al. 2019). Each gene was recombined into the destination *Xenopus* (*X. laevis*) oocyte expression vector, pGEMHE-DEST (Shelden et al. 2009), using LR Clonase Recombinase (Life Technologies) according to the manufacturer's protocol. Gene sequences were confirmed by Sanger sequencing (AGRF, Westmead, NSW, Australia). Thereafter, plasmids were linearized with the *NheI* restriction enzyme (NEB, Ipswich, MA, USA) to transcribe complementary RNA (cRNA) driven by the T7 promoter using the Ambion mMessage mMachine kit (Life Technologies) according to the manufacturer's protocol.

For heterologous expression in yeast (*S. cerevisiae*), *Lr67* alleles were sub-cloned from pENTR1A into the pDR196 yeast vector (Rentsch et al. 1995), or pDR196T vector (Milne et al. 2019) for co-expression, using EcoRI and XhoI restriction sites. Constructs are detailed in Supplemental Table S3. Site-directed mutants were produced after cloning into pENTR1A using the primers in Supplemental Table S2 and protocol above, and then subcloned using flanking restriction sites into pDR196. Yeast expression constructs were transformed into yeast as described (Dohmen et al. 1991), at least three colonies were selected as independent transformation events (biological replicates). Colonies were cultured in synthetic dropout medium lacking uracil (SDura<sup>-</sup>; 6.72 g/L yeast nitrogen base with ammonium sulfate, 0.96 g/L yeast synthetic dropout medium without uracil, 2% w/v maltose), plasmids were rescued from yeast as described using the QIAprep Miniprep Kit (QIAGEN, Chadstone Centre, VIC, Australia—User developed protocol: Isolation of plasmid DNA from yeast), transformed to *Escherichia coli* and sequences were confirmed by Sanger sequencing (AGRF).

### Expression in oocytes, radiolabeled uptake, and TEVC experiments

Stage V–VI *Xenopus* oocytes were selected and injected with 46 ng of cRNA or an equal volume (46 nL) of RNA-free water and incubated in Frog Ringer solution supplemented with antibiotics (96 mM NaCl, 2 mM KCl, 1 mM MgCl<sub>2</sub>, 0.6 mM CaCl<sub>2</sub>, 5% v/v horse serum, 100 units/mL penicillin, 1 mg/mL streptomycin, 0.5 mg/mL tetracycline, HEPES–NaOH pH 7.6) at 18 °C prior to experimentation. <sup>36</sup>Cl<sup>-</sup> uptake was performed 2 dpi and oocytes were incubated in Frog Ringer solution at pH 5.5 without antibiotics. Water, *Lr67sus*, *Lr67res*, and *TmClC-0* injected oocytes were incubated at room temperature in Frog Ringer solution containing H<sub>2</sub>[<sup>36</sup>Cl<sup>-</sup>]. Oocytes were washed three times by pipetting into 2 mL of ice-cold Frog Ringer solution lacking <sup>36</sup>Cl<sup>-</sup>. [<sup>14</sup>C]-glucose uptakes were performed identically to <sup>36</sup>Cl<sup>-</sup> uptakes but *Lr67sus*, *Lr67res*, and water-injected oocytes at 2 dpi were incubated for 1 h in 115 mM NaCl MES-Tris pH 5 Ringer solution containing 11.4 μM [<sup>14</sup>C]-glucose and washes were performed using ice-cold 115 mM NaCl MES-Tris pH 5 Ringer solution supplemented with 1 mM glucose. Each oocyte was placed in a separate scintillation vial, dissolved in 0.1% v/v nitric acid and 4 mL Optima Gold XR scintillant (Perkin Elmer, Glen Waverley, VIC, Australia) was added prior to counting for 2 min using a Liquid Scintillation Counter (LS6500; Beckman Coulter, Lane Cove, NSW, Australia).

Glucose transport of *Lr67sus* was measured using 2 dpi oocytes that were placed in a recording bath and perfused with a modified Na-Ringer solution (MES-Tris Ringer; 115 mM NaCl, 2 mM KCl, 1.8 mM CaCl<sub>2</sub>, 1 mM MgCl<sub>2</sub>, 5 mM MES-Tris at appropriate pH) (Sivitz et al. 2007). Recording pipettes, 3 M KCl filled and ~1 MΩ resistance, measured

currents using the TEVC technique as described (Sivitz et al. 2005). An Axon Instruments GeneClamp 500 amplifier (Molecular Devices, San Jose, CA, USA) was used for TEVC measurements. Pulses were applied for 203 ms at voltages from –140 to 40 mV in 20 mV increments. Steady-state currents are presented as the mean current between 150 and 200 ms following the onset of voltage pulses. Raw trace data is presented in Supplemental Figs. S7 to S9. Substrate-dependent currents were obtained by subtracting an averaged background current before and after the provision of substrate. Solution osmolarities were adjusted using mannitol to 240 to 260 mOsmol kg<sup>-1</sup> using a Wescor vapor pressure osmometer. Due to the magnitude of currents obtained in *Lr67res* oocytes and deterioration of oocytes at 2 dpi, measurements were carried out 1 dpi and presented as *I*–*V* curves. Glucose induced currents by *Lr67sus* were detectable at this time point and were observed to increase between 1 and 3 dpi. Ringer solution was as described unless indicated. Agar bridges were used as bath electrodes when experiments were performed that altered Cl<sup>-</sup> concentration or substituted Cl<sup>-</sup> for other ions. For phlorizin inhibition experiments, phlorizin was first dissolved in DMSO and added to MES-Tris Ringer at pH 5, to a final concentration of 2 mM phlorizin and 1% v/v DMSO. The control solution lacking phlorizin also contained the same concentration of DMSO and was deemed to not have an impact on *Lr67res* currents.

### Quantification of oocyte ion content

Water, *Lr67sus*, and *Lr67res*-injected oocytes incubated at 18 °C in Frog Ringer with antibiotics were sampled 48 h after injection. Two oocytes were pooled per sample and oocytes from two frogs were sampled. Oocytes were washed twice with Milli-Q water which was removed by pipetting. Oocytes were frozen at –20 °C, thawed and digested in 100 μL 0.1 M nitric acid at 42 °C for 2 h before adjusting total volume to 1 mL with Milli-Q water. Debris was removed by centrifugation and the clarified supernatant was diluted for measurement on an Atomic Absorption Spectrometer (AA-7000F; Shimadzu, North Plympton, SA, Australia). Standard curves were prepared with commercial standards for Na<sup>+</sup> and K<sup>+</sup> (Sigma–Aldrich, North Ryde, NSW, Australia) and clarified supernatants were diluted with Milli-Q water accordingly to fit the range of each standard curve. Ion concentration was calculated using 1 μL as the oocyte volume (Kelly et al. 1995).

### Measurement of oocyte cytosolic pH and membrane potential

Cytosolic pH changes were monitored using a proton sensitive microelectrode whilst membrane potential changes were monitored using a voltage electrode (electrodes were prepared as described; Bose et al. 2013). Each oocyte was placed in a recording bath submerged in a modified Na-Ringer solution at pH 7.6 or 4.5 (±1 mM glucose) that was circulated by a peristaltic pump for ~5 min after

solution change before the flow was stopped. Membrane potential and pH measurements were recorded constantly for approximately 60 min per oocyte using the microelectrode ion flux estimation (MIFE) (University of Tasmania, Hobart, Australia) system.

### Yeast uptake assays

Yeast [ $^{14}\text{C}$ ]glucose uptake experiments were performed as described (Milne et al. 2017). Briefly, yeast were grown in liquid SDura<sup>-</sup> (or SDura<sup>-</sup> trp<sup>-</sup> for co-transformed yeast) medium containing 2% w/v maltose overnight to an OD<sub>600</sub> of 0.6 to 1.0. Yeast were collected via centrifugation, washed and resuspended to an OD of 2.0 in 25 mM MES/HEPES buffer. Yeast were energized with 100 mM ethanol 1 min prior to addition of 100  $\mu\text{M}$  glucose solution containing 11.1 KBq [ $^{14}\text{C}$ ]glucose, followed by a 4-min incubation at 30 °C on a shaking platform. Yeast were collected onto a glass microfibre filter using a vacuum, washed three times with ice-cold 100  $\mu\text{M}$  glucose solution and placed into a scintillation vial with 4 mL Ultima Gold scintillant (Perkin Elmer) overnight prior to counting for 2 min using a Tricarb 2810 TR Liquid Scintillation Counter (Perkin Elmer).

### Statistical analysis

Statistical analyses (*F*-test to confirm equal variances, two-tailed *T*-test in Fig. 6A) were performed using Prism software (GraphPad, San Diego, CA, USA) and are described in figure captions as appropriate. Detailed statistical results are presented in Supplemental Table S4.

### Accession numbers

NCBI accession numbers of sequences used in this study are listed. *Lr67sus*, MV144992.1; *Lr67res*, KR604817.2; *Lr34sus*, HL100988.1; *Lr34res*, XM\_044586927.1; *TmCLC-0*, X56758.1.

### Supplemental data

The following materials are available in the online version of this article.

**Supplemental Figure S1.** *Lr67sus* glucose-dependent currents in *Xenopus* oocytes.

**Supplemental Figure S2.** Effects of external pH change on *Xenopus* oocyte cytosolic pH.

**Supplemental Figure S3.** Current–voltage relationships of water-injected control oocytes.

**Supplemental Figure S4.** Current–voltage relationship of oocytes treated with phlorizin.

**Supplemental Figure S5.** Membrane potential of water-injected control oocytes and *TmCLC-0* oocytes as bathing solution pH was changed.

**Supplemental Figure S6.** Multiple sequence alignment highlighting sequence conservation of *STP13* from various plant species.

**Supplemental Figure S7.** Raw TEVC traces obtained for *Lr67sus*, *Lr67res*, and water-injected oocytes.

**Supplemental Figure S8.** Representative raw TEVC trace data for *Lr67res*, water-injected oocytes and a comparison of *Lr34* and *Lr67* alleles.

**Supplemental Figure S9.** Representative raw TEVC trace data for *Lr67res*, *TmCLC-0*, and *Lr67res* LOR mutants.

**Supplemental Table S1.** Summary of reversal potential values for *Lr67res* and water-injected oocytes along with reversal potential shifts observed when oocyte bathing solution was substituted from 115 mM NaCl to a specified solution.

**Supplemental Table S2.** Primers used in this study.

**Supplemental Table S3.** Amplified and synthesized fragments and constructs used in this study.

**Supplemental Table S4.** Statistical analyses used in this study.

### Acknowledgments

The authors wish to thank Dr. Crystal Wu for kindly providing *TmCLC-0* cRNA; Dr. Peter Dodds, Prof. Matthew Gilliam, Dr. Caitlin Byrt, Dr. Sunita Ramesh, Dr. Megan Shelden, Dr. Stefanie Wege, Dr. Jiaen Qiu, Dr. Samantha McGaughey, and Wendy Sullivan for useful discussions and/or technical assistance. We thank Prof. Wolf Frommer for reviewing an earlier draft of this paper.

### Author contributions

R.J.M. and K.E.D. contributed to all experimental work and drafted the manuscript. R.J.M., K.E.D., and J.B. conducted oocyte experiments. R.J.M. conducted yeast experiments. R.J.M., K.E.D., J.B., A.R.A., P.R.R., S.D.T., and E.S.L. conceived experimental plans. All authors commented on draft and approved the manuscript.

### Funding

This work was supported by a Commonwealth Scientific and Industrial Research Organisation (CSIRO) Research Plus Postdoctoral Fellowship (R.J.M.), Bill and Melinda Gates Foundation Grant OPP1131636 (K.E.D., J.Z., E.S.L.), Australian Research Council Discovery Early Career Researcher Award DE170100346 (J.B.), and Australian Research Council Centre of Excellence CE140100008 (S.D.T.).

*Conflict of interest statement.* All authors declare no conflict of interest.

### Data availability

The original data that support the findings of this study are available from the corresponding author upon request.

### References

Bavnhøj L, Paulsen PA, Flores-Canales JC, Schiøtt B, Pedersen BP. Molecular mechanism of sugar transport in plants unveiled by

- structures of glucose/H<sup>+</sup> symporter STP10. *Nat Plants*. 2021;7(10):1409–1419. <https://doi.org/10.1038/s41477-021-00992-0>
- Bi G, Su M, Li N, Liang Y, Dang S, Xu J, Hu M, Wang J, Zou M, Deng Y, et al.** The ZAR1 resistosome is a calcium-permeable channel triggering plant immune signaling. *Cell*. 2021;184(13):3528–3541.e3512. <https://doi.org/10.1016/j.cell.2021.05.003>
- Boni R, Chauhan H, Hensel G, Roulin A, Sucher J, Kumlehn J, Brunner S, Krattinger SG, Keller B.** Pathogen-inducible Ta-Lr34res expression in heterologous barley confers disease resistance without negative pleiotropic effects. *Plant Biotechnol J*. 2018;16(1):245–253. <https://doi.org/10.1111/pbi.12765>
- Borre L, Kanner BI.** Arginine 445 controls the coupling between glutamate and cations in the neuronal transporter EAAC-1. *J Biol Chem*. 2004;279(4):2513–2519. <https://doi.org/10.1074/jbc.M311446200>
- Bose J, Xie Y, Shen W, Shabala S.** Haem oxygenase modifies salinity tolerance in Arabidopsis by controlling K<sup>+</sup> retention via regulation of the plasma membrane H<sup>+</sup>-ATPase and by altering SOS1 transcript levels in roots. *J Exp Bot*. 2013;64(2):471–481. <https://doi.org/10.1093/jxb/ers343>
- Bruce LJ, Robinson H C, Guizouarn H, Borgese F, Harrison P, King M-J, Goede JS, Coles SE, Gore DM, Lutz HU, et al.** Monovalent cation leaks in human red cells caused by single amino-acid substitutions in the transport domain of the band 3 chloride-bicarbonate exchanger, AE1. *Nat Genet*. 2005;37(11):1258. <https://doi.org/10.1038/ng1656>
- Custódio TF, Paulsen PA, Frain KM, Pedersen BP.** Structural comparison of GLUT1 to GLUT3 reveal transport regulation mechanism in sugar porter family. *Life Sci Alliance*. 2021;4(4):e202000858. <https://doi.org/10.26508/lsa.202000858>
- Dohmen RJ, Strasser AW, Honer CB, Hollenberg CP.** An efficient transformation procedure enabling long-term storage of competent cells of various yeast genera. *Yeast*. 1991;7(7):691–692. <https://doi.org/10.1002/yea.320070704>
- Ellis JG, Lagudah ES, Spielmeier W, Dodds PN.** The past, present and future of breeding rust resistant wheat. *Front Plant Sci*. 2014;5:641. <https://doi.org/10.3389/fpls.2014.00641>
- Gear ML, McPhillips ML, Patrick JW, McCurdy DW.** Hexose transporters of tomato: molecular cloning, expression analysis and functional characterization. *Plant Mol Biol*. 2000;44(5):687–697. <https://doi.org/10.1023/A:1026578506625>
- Greene EA, Codomo CA, Taylor NE, Henikoff JG, Till BJ, Reynolds SH, Enns LC, Burtner C, Johnson JE, Odden AR.** Spectrum of chemically induced mutations from a large-scale reverse-genetic screen in Arabidopsis. *Genetics*. 2003;164(2):731–740. <https://doi.org/10.1093/genetics/164.2.731>
- Guo W, Zuo Z, Cheng X, Sun J, Li H, Li L, Qiu J-L.** The chloride channel family gene CLCd negatively regulates pathogen-associated molecular pattern (PAMP)-triggered immunity in Arabidopsis. *J Exp Bot*. 2014;65(4):1205–1215. <https://doi.org/10.1093/jxb/ert484>
- Gupta M, Dubey S, Jain D, Chandran D.** The Medicago truncatula sugar transport protein 13 and its Lr67res-like variant confer powdery mildew resistance in legumes via defense modulation. *Plant Cell Physiol*. 2021;62(4):650–667. <https://doi.org/10.1093/pcp/pcab021>
- Han B, Jiang Y, Cui G, Mi J, Roelfsema MRG, Mouille G, Sechet J, Al-Babili S, Aranda M, Hirt H.** CATION-CHLORIDE CO-TRANSPORTER 1 (CCC1) mediates plant resistance against *Pseudomonas syringae*1. *Plant Physiol*. 2019;182(2):1052–1065. <https://doi.org/10.1104/pp.19.01279>
- Hayes MA, Davies C, Dry IB.** Isolation, functional characterization, and expression analysis of grapevine (*Vitis vinifera* L.) hexose transporters: differential roles in sink and source tissues. *J Exp Bot*. 2007;58(8):1985–1997. <https://doi.org/10.1093/jxb/erm061>
- Hayes MA, Feechan A, Dry IB.** Involvement of abscisic acid in the coordinated regulation of a stress-inducible hexose transporter (VvHT5) and a cell wall invertase in grapevine in response to biotrophic fungal infection. *Plant Physiol*. 2010;153(1):211–221. <https://doi.org/10.1104/pp.110.154765>
- Huai B, Yang Q, Wei X, Pan Q, Kang Z, Liu J.** TaSTP13 contributes to wheat susceptibility to stripe rust possibly by increasing cytoplasmic hexose concentration. *BMC Plant Biol*. 2020;20(1):49. <https://doi.org/10.1186/s12870-020-2248-2>
- Huerta-Espino J, Singh R, Crespo-Herrera LA, Villaseñor-Mir HE, Rodriguez-Garcia MF, Dreisigacker S, Barcenas-Santana D, Lagudah E.** Adult plant slow rusting genes confer high levels of resistance to rusts in bread wheat cultivars from Mexico. *Front Plant Sci*. 2020;11:824. <https://doi.org/10.3389/fpls.2020.00824>
- Jacob P, Kim NH, Wu F, El-Kasmi F, Chi Y, Walton WG, Furzer OJ, Lietzan AD, Sunil S, Kempthorn K, et al.** Plant “helper” immune receptors are Ca<sup>2+</sup>-permeable nonselective cation channels. *Science*. 2021;373(6553):420–425. <https://doi.org/10.1126/science.abg7917>
- Jentsch TJ, Steinmeyer K, Schwarz G.** Primary structure of *Torpedo marmorata* chloride channel isolated by expression cloning in *Xenopus* oocytes. *Nature*. 1990;348(6301):510–514. <https://doi.org/10.1038/348510a0>
- Kelly SM, Butler JP, Macklem PT.** Control of cell volume in oocytes and eggs from *Xenopus laevis*. *Comp Biochem Physiol A Physiol*. 1995;111(4):681–691. [https://doi.org/10.1016/0300-9629\(95\)00046-A](https://doi.org/10.1016/0300-9629(95)00046-A)
- Kollist H, Jossier M, Laanemets K, Thomine S.** Anion channels in plant cells. *FEBS J*. 2011;278(22):4277–4292. <https://doi.org/10.1111/j.1742-4658.2011.08370.x>
- Kolmer JA, Lagudah ES, Lillemo M, Lin M, Bai G.** The Lr46 gene conditions partial adult-plant resistance to stripe rust, stem rust, and powdery mildew in thatcher wheat. *Crop Sci*. 2015;55(6):2557–2565. <https://doi.org/10.2135/cropsci2015.02.0082>
- Krattinger SG, Kang J, Bräunlich S, Boni R, Chauhan H, Selter LL, Robinson MD, Schmid MW, Wiederhold E, Hensel G, et al.** Abscisic acid is a substrate of the ABC transporter encoded by the durable wheat disease resistance gene Lr34. *New Phytol*. 2019;223(2):853–866. <https://doi.org/10.1111/nph.15815>
- Krattinger SG, Lagudah ES, Spielmeier W, Singh RP, Huerta-Espino J, McFadden H, Bossolini E, Selter LL, Keller B.** A putative ABC transporter confers durable resistance to multiple fungal pathogens in wheat. *Science*. 2009;323(5919):1360–1363. <https://doi.org/10.1126/science.1166453>
- Krattinger SG, Sucher J, Selter LL, Chauhan H, Zhou B, Tang M, Upadhyaya NM, Mieulet D, Guiderdoni E, Weidenbach D, et al.** The wheat durable, multipathogen resistance gene Lr34 confers partial blast resistance in rice. *Plant Biotechnol J*. 2016;14(5):1261–1268. <https://doi.org/10.1111/pbi.12491>
- Lemonnier P, Gaillard C, Veillet F, Verbeke J, Lemoine R, Coutos-Thevenot P, La Camera S.** Expression of Arabidopsis sugar transport protein STP13 differentially affects glucose transport activity and basal resistance to *Botrytis cinerea*. *Plant Mol Biol*. 2014;85(4–5):473–484. <https://doi.org/10.1007/s11103-014-0198-5>
- Li Y, Li W, Li J.** The CRISPR/Cas9 revolution continues: from base editing to prime editing in plant science. *J Genet Genomics*. 2021;48(8):661–670. <https://doi.org/10.1016/j.jgg.2021.05.001>
- Liu K-H, Huang C-Y, Tsay Y-F.** CHL1 is a dual-affinity nitrate transporter of Arabidopsis involved in multiple phases of nitrate uptake. *Plant Cell*. 1999;11(5):865–874. <https://doi.org/10.1105/tpc.11.5.865>
- Liu Y, Maierhofer T, Rybak K, Sklenar J, Breakspear A, Johnston MG, Fliegmann J, Huang S, Roelfsema MRG, Felix G, et al.** Anion channel SLAH3 is a regulatory target of chitin receptor-associated kinase PBL27 in microbial stomatal closure. *Elife*. 2019;8:e44474. <https://doi.org/10.7554/eLife.44474>
- Liu K-H, Tsay Y-F.** Switching between the two action modes of the dual-affinity nitrate transporter CHL1 by phosphorylation. *EMBO J*. 2003;22(5):1005–1013. <https://doi.org/10.1093/emboj/cdg118>
- Martial S, Guizouarn H, Gabillat N, Pellissier B, Borgese F.** Consequences of point mutations in trout anion exchanger 1 (tAE1) transmembrane domains: evidence that tAE1 can behave as a chloride channel. *J Cell Physiol*. 2006;207(3):829–835. <https://doi.org/10.1002/jcp.20631>
- Meredith D.** Site-directed mutation of arginine 282 to glutamate uncouples the movement of peptides and protons by the rabbit

- proton-peptide cotransporter PepT1. *J Biol Chem*. 2004;**279**(16): 15795–15798. <https://doi.org/10.1074/jbc.M313922200>
- Milne RJ, Dibley KE, Lagudah ES.** Yeast as a heterologous system to functionally characterize a multiple rust resistance gene that encodes a hexose transporter. In: **Periyannan S**, editor. *Wheat rust diseases: methods and protocols*. New York (NY): Springer New York; 2017. p. 265–274
- Milne RJ, Dibley KE, Schnippenkoetter WH, Mascher M, Lui AC, Wang L, Lo C, Ashton AR, Ryan PR, Lagudah E.** The wheat *Lr67* gene from the sugar transport protein 13 family confers multipathogen resistance in barley. *Plant Physiol*. 2019;**179**(4):1285–1297. <https://doi.org/10.1104/pp.18.00945>
- Moore JW, Herrera-Foessel S, Lan C, Schnippenkoetter W, Ayliffe M, Huerta-Espino J, Lillemo M, Viccars L, Milne R, Periyannan S, et al.** A recently evolved hexose transporter variant confers resistance to multiple pathogens in wheat. *Nat Genet*. 2015;**47**(12):1494–1498. <https://doi.org/10.1038/ng.3439>
- Munns R, James RA, Xu B, Athman A, Conn SJ, Jordans C, Byrt CS, Hare RA, Tyerman SD, Tester M, et al.** Wheat grain yield on saline soils is improved by an ancestral Na<sup>+</sup> transporter gene. *Nat Biotechnol*. 2012;**30**(4):360. <https://doi.org/10.1038/nbt.2120>
- Nørholm MHH, Nour-Eldin HH, Brodersen P, Mundy J, Halkier BA.** Expression of the Arabidopsis high-affinity hexose transporter STP13 correlates with programmed cell death. *FEBS Lett*. 2006;**580**(9): 2381–2387. <https://doi.org/10.1016/j.febslet.2006.03.064>
- Paulsen PA, Custódio TF, Pedersen BP.** Crystal structure of the plant symporter STP10 illuminates sugar uptake mechanism in monosaccharide transporter superfamily. *Nat Commun*. 2019;**10**(1):407. <https://doi.org/10.1038/s41467-018-08176-9>
- Pretorius ZA, Singh RP, Wagoire WW, Payne TS.** Detection of virulence to wheat stem rust resistance gene *Sr31* in *Puccinia graminis* f. sp. *tritici* in Uganda. *Plant Dis*. 2000;**84**(2):203–203. <https://doi.org/10.1094/PDIS.2000.84.2.203B>
- Qin X, Boron WF.** Mutation of a single amino acid converts the human water channel aquaporin 5 into an anion channel. *Am J Physiol Cell Physiol*. 2013;**305**(6):C663–C672. <https://doi.org/10.1152/ajpcell.00129.2013>
- Reinders A, Sivitz AB, Starker CG, Gantt JS, Ward JM.** Functional analysis of LjSUT4, a vacuolar sucrose transporter from *Lotus japonicus*. *Plant Mol Biol*. 2008;**68**(3): 289. <https://doi.org/10.1007/s11103-008-9370-0>
- Rentsch D, Laloi M, Rouhara I, Schmelzer E, Delrot S, Frommer WB.** NTR1 encodes a high affinity oligopeptide transporter in Arabidopsis. *FEBS Lett*. 1995;**370**(3):264–268. [https://doi.org/10.1016/0014-5793\(95\)00853-2](https://doi.org/10.1016/0014-5793(95)00853-2)
- Risk JM, Selter LL, Chauhan H, Krattinger SG, Kumlehn J, Hensel G, Viccars LA, Richardson TM, Buesing G, Troller A, et al.** The wheat *Lr34* gene provides resistance against multiple fungal pathogens in barley. *Plant Biotechnol J*. 2013;**11**(7):847–854. <https://doi.org/10.1111/pbi.12077>
- Sasaki J, Brown L, Chon Y, Kandori H, Maeda A, Needleman R, Lanyi J.** Conversion of bacteriorhodopsin into a chloride ion pump. *Science*. 1995;**269**(5220):73–75. <https://doi.org/10.1126/science.7604281>
- Schnippenkoetter W, Lo C, Liu G, Dibley K, Chan WL, White J, Milne R, Zwart A, Kwong E, Keller B, et al.** The wheat *Lr34* multipathogen resistance gene confers resistance to anthracnose and rust in sorghum. *Plant Biotechnol J*. 2017;**15**(11):1387–1396. <https://doi.org/10.1111/pbi.12723>
- Shelden MC, Howitt SM, Kaiser BN, Tyerman SD.** Identification and functional characterisation of aquaporins in the grapevine, *Vitis vinifera*. *Funct Plant Biol*. 2009;**36**(12):1065–1078. <https://doi.org/10.1071/FP09117>
- Singh RP, Mujeeb-Kazi A, Huerta-Espino J.** *Lr46*: a gene conferring slow-rusting resistance to leaf rust in wheat. *Phytopathology*. 1998;**88**(9):890–894. <https://doi.org/10.1094/PHYTO.1998.88.9.890>
- Sivitz AB, Reinders A, Johnson ME, Krentz AD, Grof CP, Perroux JM, Ward JM.** Arabidopsis sucrose transporter AtSUC9. High-affinity transport activity, intragenic control of expression, and early flowering mutant phenotype. *Plant Physiol*. 2007;**143**(1):188–198. <https://doi.org/10.1104/pp.106.089003>
- Sivitz AB, Reinders A, Ward JM.** Analysis of the transport activity of barley sucrose transporter HvSUT1. *Plant Cell Physiol*. 2005;**46**(10): 1666–1673. <https://doi.org/10.1093/pcp/pci182>
- Skoppek CI, Punt W, Heinrichs M, Ordon F, Wehner G, Boch J, Streubel J.** The barley HvSTP13GR mutant triggers resistance against biotrophic fungi. *Mol Plant Pathol*. 2022;**23**(2):278–290. <https://doi.org/10.1111/mpp.13161>
- Slewinski TL.** Diverse functional roles of monosaccharide transporters and their homologs in vascular plants: a physiological perspective. *Mol Plant*. 2011;**4**(4):641–662. <https://doi.org/10.1093/mp/ssr051>
- Spielmeyer W, Mago R, Wellings C, Ayliffe M.** *Lr67* and *Lr34*rust resistance genes have much in common—they confer broad spectrum resistance to multiple pathogens in wheat. *BMC Plant Biol*. 2013;**13**(1): 96. <https://doi.org/10.1186/1471-2229-13-96>
- Sucher J, Boni R, Yang P, Rogowsky P, Büchner H, Kastner C, Kumlehn J, Krattinger SG, Keller B.** The durable wheat disease resistance gene *Lr34* confers common rust and northern corn leaf blight resistance in maize. *Plant Biotechnol J*. 2017;**15**(4):489–496. <https://doi.org/10.1111/pbi.12647>
- Sun Y, Reinders A, LaFleur KR, Mori T, Ward JM.** Transport activity of rice sucrose transporters OsSUT1 and OsSUT5. *Plant Cell Physiol*. 2010;**51**(1):114–122. <https://doi.org/10.1093/pcp/pcp172>
- Sun L, Zeng X, Yan C, Sun X, Gong X, Rao Y, Yan N.** Crystal structure of a bacterial homologue of glucose transporters GLUT1–4. *Nature*. 2012;**490**(7420):361. <https://doi.org/10.1038/nature11524>
- Till BJ, Cooper J, Tai TH, Colowit P, Greene EA, Henikoff S, Comai L.** Discovery of chemically induced mutations in rice by TILLING. *BMC Plant Biol*. 2007;**7**(1):1–12. <https://doi.org/10.1186/1471-2229-7-19>
- Uozumi N, Kim EJ, Rubio F, Yamaguchi T, Muto S, Tsuboi A, Bakker EP, Nakamura T, Schroeder JI.** The Arabidopsis *HKT1* gene homolog mediates inward Na<sup>+</sup> currents in *Xenopus laevis* oocytes and Na<sup>+</sup> uptake in *Saccharomyces cerevisiae*. *Plant Physiol*. 2000;**122**(4): 1249–1260. <https://doi.org/10.1104/pp.122.4.1249>
- Wang Y-Y, Hsu P-K, Tsay Y-F.** Uptake, allocation and signaling of nitrate. *Trends Plant Sci*. 2012;**17**(8):458–467. <https://doi.org/10.1016/j.tplants.2012.04.006>
- Weber W.** Ion currents of *Xenopus laevis* oocytes: state of the art. *Biochim Biophys Acta*. 1999;**1421**(2):213–233. [https://doi.org/10.1016/S0005-2736\(99\)00135-2](https://doi.org/10.1016/S0005-2736(99)00135-2)
- Weber YG, Storch A, Wuttke TV, Brockmann K, Kempfle J, Maljevic S, Margari L, Kamm C, Schneider SA, Huber SM, et al.** GLUT1 mutations are a cause of paroxysmal exertion-induced dyskinesias and induce hemolytic anemia by a cation leak. *J Clin Invest*. 2008;**118**(6):2157–2168. <https://doi.org/10.1172/JCI34438>
- Wisedchaisri G, Park M-S, Iadanza MG, Zheng H, Gonen T.** Proton-coupled sugar transport in the prototypical major facilitator superfamily protein Xyle. *Nat Commun*. 2014;**5**(1):4521. <https://doi.org/10.1038/ncomms5521>
- Yamada K, Kanai M, Osakabe Y, Ohiraki H, Shinozaki K, Yamaguchi-Shinozaki K.** Monosaccharide absorption activity of Arabidopsis roots depends on expression profiles of transporter genes under high salinity conditions. *J Biol Chem*. 2011;**286**(50): 43577–43586. <https://doi.org/10.1074/jbc.M111.269712>
- Yamada K, Saijo Y, Nakagami H, Takano Y.** Regulation of sugar transporter activity for antibacterial defense in Arabidopsis. *Science*. 2016;**354**(6318):1427–1430. <https://doi.org/10.1126/science.aah5692>